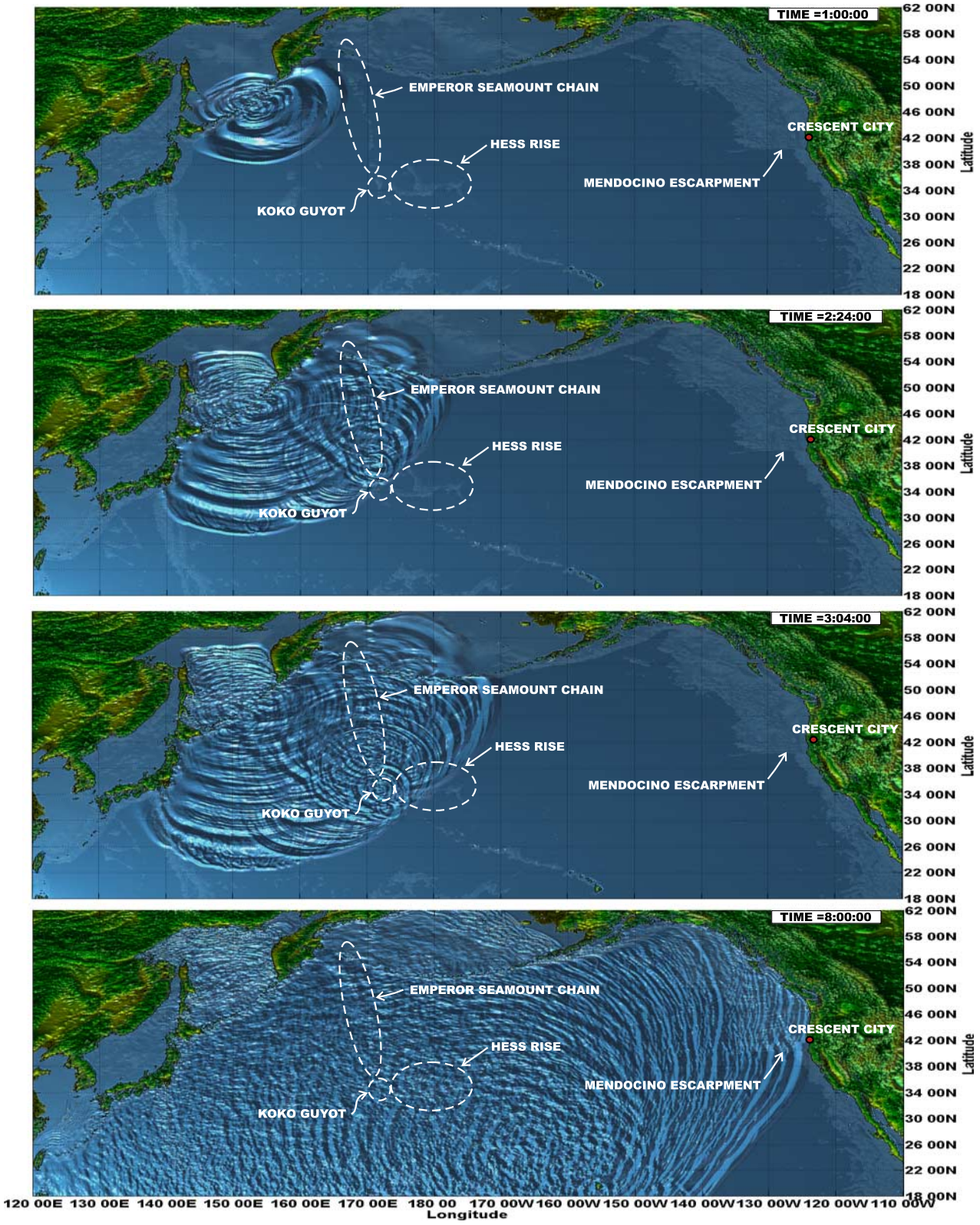

Figure 4. Snapshots of Kuril tsunami development in the northern Pacific. Large bathymetric features, like Koko Guyot and Hess Rise, scatter tsunami in directions different from the incident direction. Time is given from the tsunami onset.

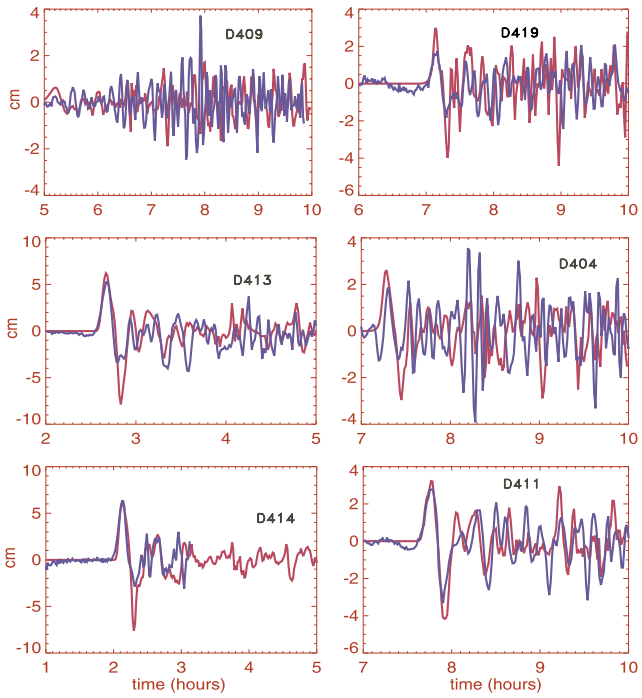

Figure 5. Sea level during Kuril Tsunami of 15 November 2006. Blue denotes recorded by DART buoys; red denotes model computation. Time is given from the tsunami onset.

where ρ is the sea water density, $g = 9.81$ m s^{-2} is the Earth's gravity acceleration and H is the ocean depth. The energy flux vector for the progressive wave propagates in the direction given by the sign of the product of sea level times velocity and is perpendicular to the wave front.

[14] To investigate the pattern of energy trapping over the Mendocino Escarpment as shown in Figure 2, the energy flux is used in two simple experiments. Three waves of 16 minutes period each and 10 cm amplitude are sent toward the west coast of North America from the open boundary located at 150°W (Figure 7a, left). In Figure 7a (right) the wave pattern 160 min later is shown. The energy flux vectors in these figures demonstrate the strong local amplification of energy flux during wave propagation toward CC. The wave amplitude shows a corresponding strong local amplification as well. The central latitude for the amplified wave is 41°N–42°N, while the Mendocino Escarpment is located close to 40°N. Thus the center of amplification is located in the narrow range of 1–2 degrees of latitude just north from the escarpment. This result is confirmed by Figure 6 where tsunami traveling along 41°20′N shows the strongest amplification for the later arriving wave group. Experiments with various wave periods resulted in the same pattern of high amplification within a narrow latitude band just north of the Mendocino Escarpment. Obviously the energy flux pattern depicted in Figure 7a is related to the depth difference along the N-S direction when crossing the escarpment. The wave south of the escarpment travels faster than the wave on the northern side of escarpment. This difference in the phase speed causes wave refraction [*Wiegel*, 1965; *Mei et al.*, 2005] resulting in steady energy amplification and focusing toward CC. The amplification shown in Figure 6 is related to the second wave group which as we are going to demonstrate arrives from the west. The initial wave as seen from Figure 4 arrives from the northwest and does not travel along the Mendocino Escarpment for any great distance.

[15] In the second experiment three waves of 25-min period each and 10 cm amplitude are sent from the northern boundary toward the Mendocino Escarpment (Figure 7b, left). The wave pattern 110 min later is shown in Figure 7b (right). Tsunami waves cross the escarpment without amplification. The direction of wave propagation seems to play the major role in tsunami enhancement along the Mendocino Escarpment.

[16] In the above computations according to Figure 6 we have applied shorter period (16 min) for the wave arriving from the west and longer period for the wave arriving from the north (25 min). Numerical experiments with wave periods from 10 min to 60 min confirmed that the above patterns of wave propagation are independent of the wave period.

[17] From Figure 7, one can also appreciate an important property of the energy flux. While the sea level can change sign, the energy flux of the progressive wave is always aligned with the direction of wave front propagation. Thus the noisy behavior of the sea level is replaced by the steadier behavior of the energy flux. This property is important in our search for the energy incoming toward CC. To investigate energy flux traveling toward CC during the Kuril tsunami we consider a 5° box enclosing CC and calculate the energy flowing into and out of the box. The box around CC is constructed as follows. The west boundary is located at 129°W, the north boundary at 44.5°N, the south boundary at 39.5°N and the east boundary is on land. The time-dependent energy flux is averaged over the length of each boundary.

[18] The results given in Figure 8 show two distinct pulses of energy crossing the western face of the box toward CC. Within the second pulse, two maxima occur separated by 20 min time interval. Energy appears to have a period of about 6–15 min. The periodicity of the energy flux of the progressive waves is different from the sea level oscillation,

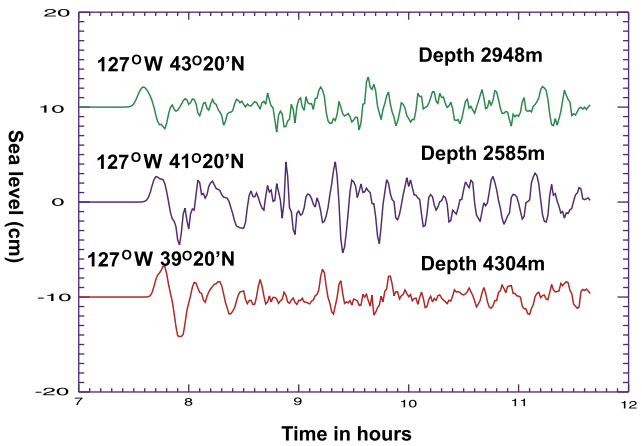

Figure 6. Time series of the tsunami waves in the proximity of Crescent City. The middle numerical gauge is located north of the Mendocino Escarpment facing Crescent City. Time is given from the tsunami onset.

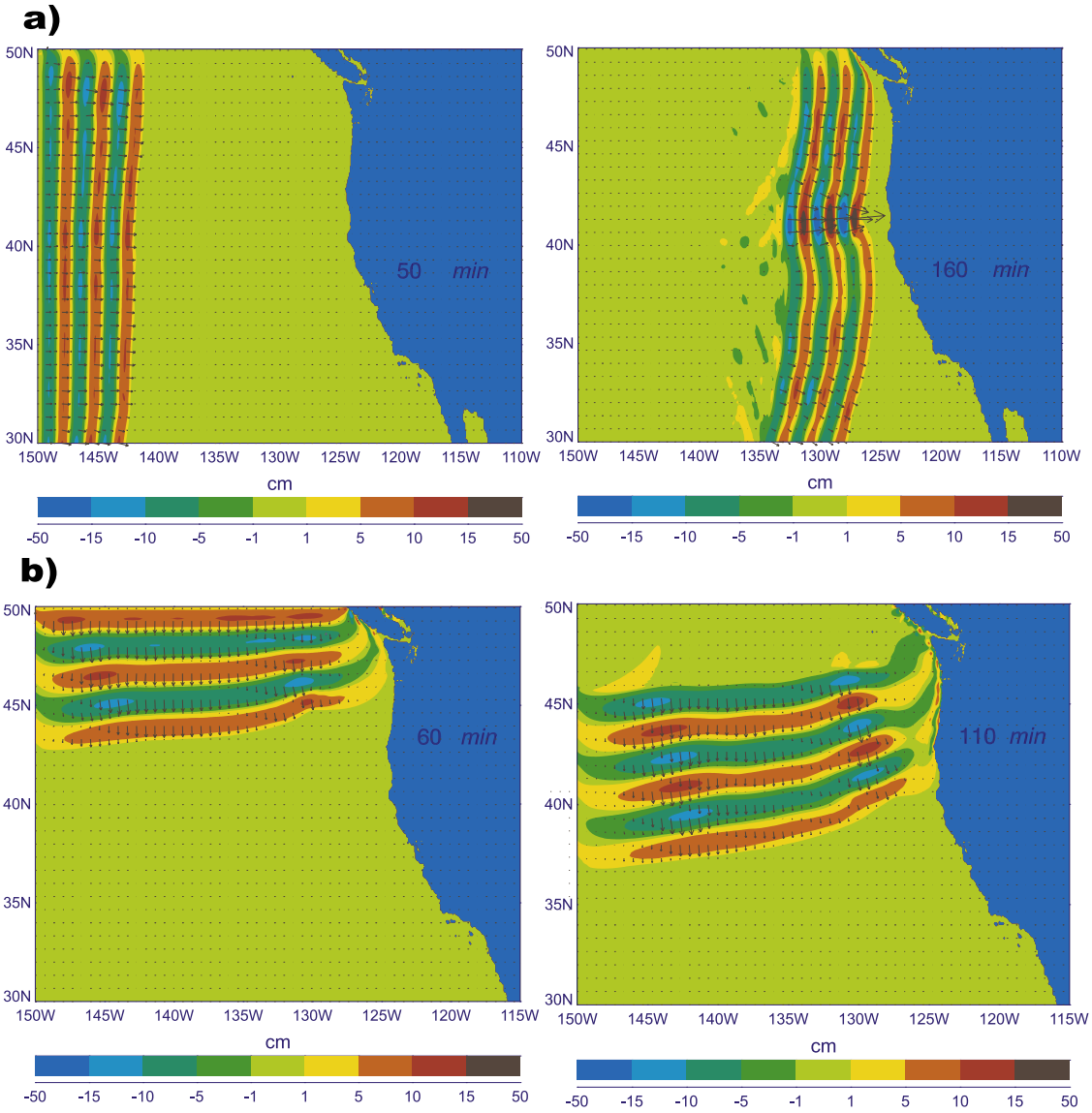

Figure 7. a) Three waves of 10 cm amplitude and 16-min period traveling parallel to the Mendocino Escarpment. (b) Three waves of 10 cm amplitude and 25-min period traveling from the north toward Mendocino Escarpment. Amplitude is given by colors. Vectors denote energy flux.

as its period of propagation is 2 times shorter than that of the sea level or velocity [*Henry and Foreman*, 2001]. It is interesting to see that there is very little reflected energy coming back across the faces of the box. This must mean that most of the incident energy is dissipated by the near shore bottom friction.

[19] Nearly the entire energy flux enters the box through the western wall. Although the first wave group propagates from the northwest (see Figure 4), the front of these waves becomes nearly parallel to the shore owing to refraction (see Figures 4 and 7b).

[20] Energy flux through faces of the box around CC can be easily applied to pinpoint the source of the second wave packet. First we simply remove from the bathymetry the Hess Rise (see Figure 3) by setting it to the depth of 5000 m. Next, the Koko Guyot is removed in the same manner. In Figure 9 the energy flux crossing the western wall is plotted; in Figure 9 (top) the Hess Rise is removed but the Koko Guyot stays unchanged and in Figure 9 (bottom) the Koko Guyot has been removed while the Hess Rise remains unchanged. For comparison the energy flux across the western face from Figure 8 is also given.

[21] The absence of Koko Guyot resulted in a restructuring of the energy flux through the western face of the box in such a way that the first maximum in the second wave group practically disappeared (Figure 9, bottom). The second maximum in this later wave group, as Figure 9 (top) shows, is related to the Hess Rise. The absence of the Hess Rise leads to energy amplification from the Koko Guyot as the Hess Rise did not scatter any longer the energy send by Koko Guyot toward CC. We can also conclude from Figure 9 that the first group of waves to arrive at CC must travel a route unobstructed by either Koko Guyot or the Hess Rise.

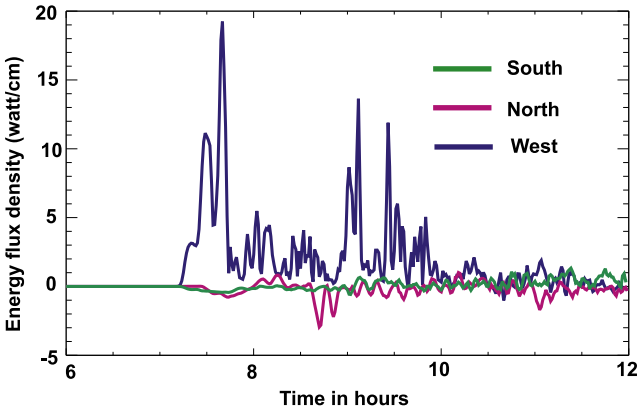

Figure 8. Energy flux through the western (blue), northern (red), and southern (green) walls of a 5° box around Crescent City.

[22] The immense influence of the Koko Guyot on tsunami signal scattering is due to its size and strong contrast between shallow and deep waters. It rises from the depth of 4750 m to within 250 m of the ocean surface [*Davies et al.*, 1972]. To further identify Koko Guyot as an important bathymetric feature, we plot in Figure 10 the energy flux vectors immediately following passage of the main energy lobe past Koko. Note the new wave front radiating from this secondary source. The Hess Rise is an elongated plateau, located to the east from Koko Guyot, with a few smaller subdomains which generally parallel the Mendocino Escarpment [*British Oceanographic Data Centre*, 2003]. Although it rises from the deep ocean plain to just 1500 m below the surface, it extends 1000 km in the E-W direction. The Hess Rise ridge like structure tends to enhance tsunami scattered from Koko Guyot and directs it toward Mendocino Escarpment; see Figure 10.

6. Spatial Resolution

[23] The latter experiments show that the strength of the second group of waves arriving at Crescent City (CC) depend strongly on bottom topography. Therefore it is important to investigate whether the numerical bottom bathymetry changes resulting from different spatial resolutions will change the predicted tsunami amplitude and phase. The influence of the magnitude of the spatial step used in the numerical model is investigated by computing the Kuril Islands tsunami generated by the same source function but with two different space steps, namely 1 and 2 arcminutes. The comparison is made for the two DART buoy locations: D413 and D411; see Figure 3.

[24] We can glean from Figure 11 that the initial signals at D413 (close to the source) and at D411 (far from the source) are unchanged when computed with either spatial resolution. Later waves, however, show phase and amplitude differences for the two space steps. Waves which follow the initial signal show differences in amplitude and phase for the computations with the different space step. These secondary waves are generated by various bathymetric features through scattering and refocusing of the initial signal. Obviously the differences in signal between the two computations originate from the different bathymetric resolutions. Small differences in bathymetry between 1 and 2 arcminutes spatial resolutions underline the importance of high-resolution bathymetry in reproducing tsunami by numerical-hydrodynamical models.

7. Discussion and Conclusions

[25] The sea level recorded in the wake of Kuril Islands tsunami of 15 November 2006 by the West Coast tidal stations and by the open ocean DART buoys show strong tsunami signal enhancement by the shallowing bathymetry (http://wcatwc.arh.noaa.gov/previous.events/11.15.2006/11-15-06.html). In a few locations along California shoreline the peak tsunami wave range leaped over 1 m (Arena Cove, 118 cm; Port San Luis, 115 cm), but again the highest range of 176 cm occurred at Crescent City (CC).

[26] The purpose of the present study was to examine and to explain amplification observed at the CC through tsunami refocusing by the distant bathymetric features. The tsunami signal at CC shows an initial wave group which was followed 2 hours later by second group of larger waves. The peculiarities in the tsunami signal attest to the scattering of the tsunami signal by various bathymetric features. The basic results from the model computations given in Figures 2 and 4 show that: (1) an amplified signal is directed toward CC and (2) it is composed of two distinct wave groups which arrive approximately from the northwest and from the west.

[27] Comparison of the model with deep ocean DART buoys shows that the model reproduces well the first group of waves. There are differences between model and mea-

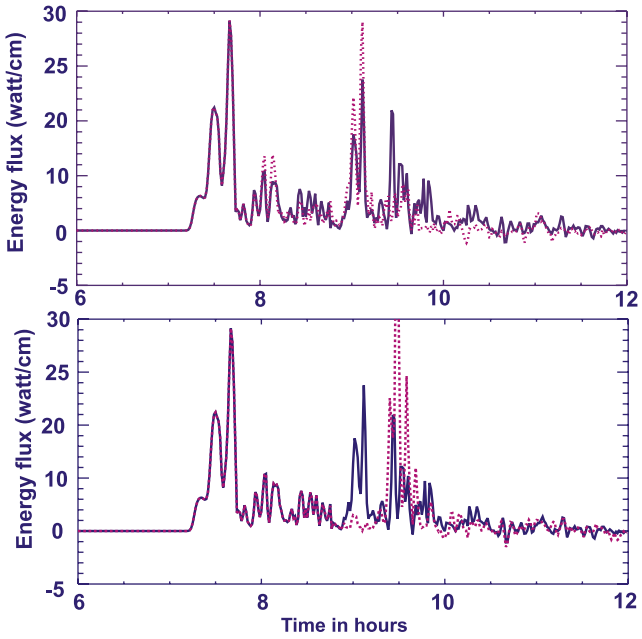

Figure 9. Energy flux through the western wall of a 5° box around Crescent City. Blue line denotes regular bathymetry. Red line denotes (top) when Hess Rise is removed from bathymetry and (bottom) when Koko Guyot is removed from bathymetry.

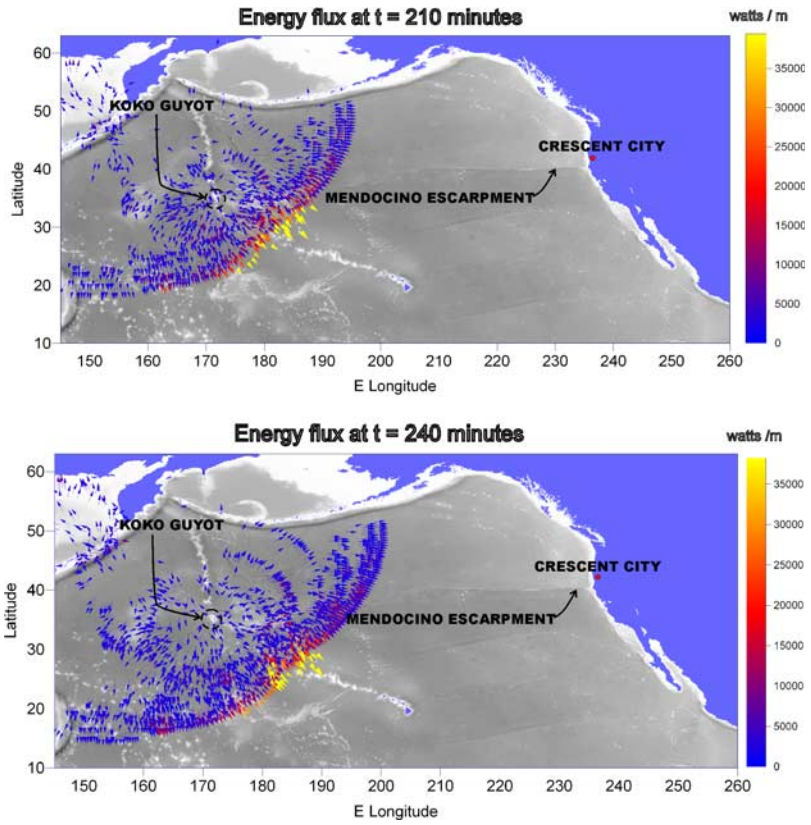

Figure 10. Energy flux vectors (top) 3.5 hours and (bottom) 4 hours after tsunami onset. Note radially expanding wave front centered on Koko Guyot.

surement with the second group, differences which often grow in time. The later arriving waves are influenced by the scattering/trapping mechanism and energy enhancement around bathymetric features as *Hebert et al.* [2001] demonstrated for the 1994 Kuril tsunami and *Kowalik et al.* [2005, 2007a] and *Titov et al.* [2005] demonstrated for the Indian Ocean Tsunami of 2004.

[28] Along with the primary source of tsunami, sea level uplift due to earthquake, the secondary sources due to scattering and refocusing complicate the process of tsunami propagation. The secondary ridge-amplified and seamount-scattered waves travel more slowly from the primary source and arrive later at distant coastal points. As a result, interactions between wave fronts derived from primary and secondary sources lead to difficulties in predicting the arrival time of the largest amplitude wave. These waves are important for tsunami prediction, warning and hazard mitigation.

[29] To investigate tsunami behavior we use energy flux. We have comprehensively tested this tool to reveal various aspects of tsunami physics [*Kowalik et al.*, 2007b] and we hope that it can serve well for tsunami prediction, warning, and hazard mitigation. Energy flux in contrast to the noisy tsunami sea level reveals uniform behavior in time and space. In addition it contains information about the directionality of the signal which is important for identification of the prominent bathymetric features as potential sources of tsunami wave refocusing. The energy flux is applied to investigate enhancement of tsunami signal and sources of the late arriving tsunami at CC. Simple numerical experiments reveal energy trapping and enhancement by the Mendocino Escarpment. These experiments define bathymetric features which scatter the tsunami signal toward CC via the Mendocino Escarpment. This escarpment seems to be efficient in delivering enhanced tsunami energy if the approaching tsunami signal travels from the west along the escarpment. To pinpoint the sources of late signals, a control box is constructed around CC and the energy flux through faces of the box is examined. The results are quite surprising, showing the key role played by two bathymetric features thousands of kilometers distant from CC (Koko Guyot and the Hess Rise) in refocusing tsunami signal toward CC. These prominent bathymetric features scattered, delayed and rerouted the tsunami signal more efficiently toward CC.

[30] As the later arriving group of waves depends strongly on the depth contrast between shallower and deeper domains surrounding bathymetric features [*Mei et al.*, 2005; *Mofjeld et al.*, 2000] it is important to consider the influence of spatial resolution on the calculated results. Presently the open ocean bathymetry is resolved with 1 arcminute spatial step. Finer resolution is not available and the 1 arcminute bathymetry in many locations (especially close to Aleutian Islands) is smoothed owing the lack of measurements. Two experiments with different spatial resolution have shown that the later arriving group of waves which is generated by tsunami/bathymetry interaction depends on the spatial resolution of the bathymetry. These

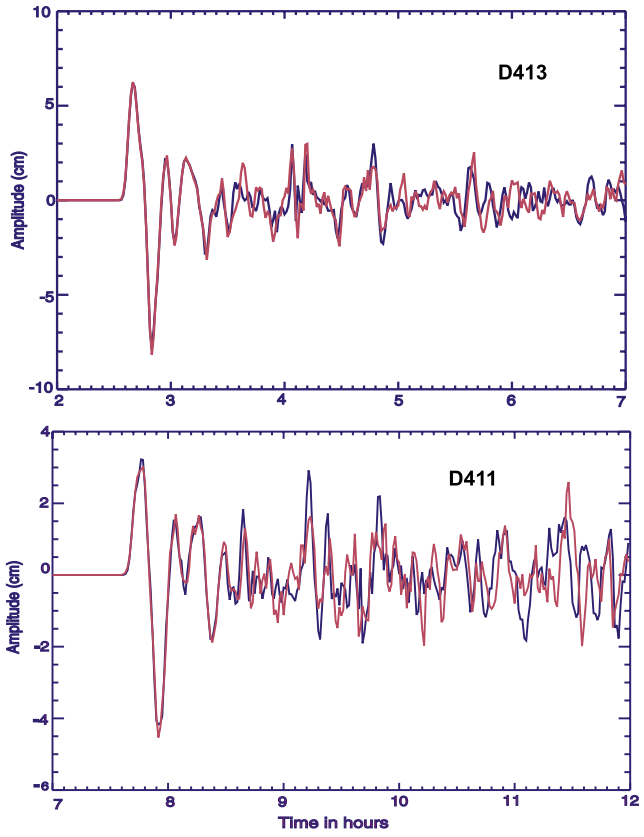

Figure 11. Sea level computed at two DART buoy locations. Blue denotes 1 arcminute spatial resolution; red denotes 2 arcminutes spatial resolution.

differences cannot be explained by numerical dispersion since neither of these spatial resolutions introduce significant dispersion. Therefore further improvement to tsunami calculations will require finer resolution of the major bathymetric features.

[31] Our investigations are based on the long wave approach. Unique measurements of currents and sea level taken by *Bricker et al.* [2007] in the wake of Kuril Islands tsunami 2006 delineate periodical motion with periods less than 10 min thus pointing toward short dispersive waves. Examination of tsunami signals (Figures 5 and 11) scattered from the bathymetric features also shows stronger influence of shorter wave periods when compared with the primary tsunami signal generated by source. Similar conclusion follows from *Horrillo et al.* [2006] numerical experiments on interaction of dispersive and nondispersive wave trains with bathymetry; the dispersive wave trains tend to generate shorter wave periods. Therefore the role of dispersive waves in the tsunami scattering will require further investigations.

[32] **Acknowledgment.** We would like to express our gratitude to reviewers for their comments and suggestions which enhanced this manuscript.

References

Bernard, E., C. Mader, G. Curtis, and K. Satake (1994), Tsunami inundation model study of Eureka and Crescent City, California, *NOAA Tech. Memo. ERL PMEL-103*, 81 pp., NOAA, Silver Spring, Md.

Bricker, J. D., S. Munger, J. R. Wells, G. Pawlak, and K. F. Cheung (2007), ADCP observations of edge waves off Oahu in the wake of the November 2006 Kuril Islands tsunami, *Geophys. Res. Lett.*, *34*, L23617, doi:10.1029/2007GL032015.

British Oceanographic Data Centre (2003), *GEBCO Digital Atlas* [CD-ROM], Disk 1, Liverpool, U.K.

Davies, T. A., P. Wilde, and D. A. Clague (1972), Koko Seamount: A major guyot at the southern end of the Emperor Seamounts, *Mar. Geol.*, *13*, 311–321.

Gill, A. E. (1982), *Atmosphere-Ocean Dynamics*, 662 pp., Academic Press, San Diego, Calif.

Gonzalez, F. I., K. Satake, E. F. Boss, and H. O. Mosfjeld (1995), Edge wave and non-trapped modes of the 25 April 1992 Cape Mendocino tsunami, *Pure Appl. Geophys.*, *144*(3/4), 409–426.

Hebert, H., P. Heinrich, F. Schindele, and A. Piatanesi (2001), Far-field simulation of tsunami propagation in the Pacific Ocean: Impact on the Marquesas Island (French Polynesia), *J. Geophys. Res.*, *106*(C5), 9161–9177.

Henry, R. F., and M. G. Foreman (2001), A representation of tidal currents based on energy flux, *Mar. Geod.*, *24*, 139–152.

Horrillo, J., Z. Kowalik, and Y. Shigihara (2006), Wave dispersion study in the Indian Ocean-Tsunami of December 26, 2004, *Mar. Geod.*, *29*, 149–166.

Imamura, F. (1996), Review of tsunami simulation with a finite difference method, in *Long-Wave Run-up Models*, edited by H. Yeah, P. Liu, and C. Synolakis, pp. 25–42, World Sci., Hackensack, N. J.

Keulegan, G. H., J. Harrison, and M. J. Mathews (1969), Theoretics in design of the proposed Crescent City harbor tsunami model, *Tech. Rep. H-69-9*, 124 pp., Waterw. Exp. Stn., U.S. Army Corps of Eng., Vicksburg, Miss.

Koshimura, S., F. Imamura, and N. Shuto (1999), Propagation of obliquely incident tsunami on a slope Part I: Amplification of tsunamis on a continental slope, *Coastal Eng. J.*, *41*(2), 151–164.

Kowalik, Z., and T. S. Murty (1993), *Numerical Modeling of Ocean Dynamics*, 481 pp., World Sci., Hackensack, N. J.

Kowalik, Z., W. Knight, T. Logan, and P. Whitmore (2005), Numerical modeling of the global tsunami: Indonesian Tsunami of 26 December 2004, *Sci. Tsunami Haz.*, *23*(1), 40–56.

Kowalik, Z., W. Knight, T. Logan, and P. Whitmore (2007a), Numerical modeling of the Indian Ocean tsunami, in *The Indian Ocean Tsunami*, edited by T. Murty, U. Aswathanarayana, and N. Nirupama, pp. 97–122, Taylor and Francis, London.

Kowalik, Z., W. Knight, T. Logan, and P. Whitmore (2007b), The tsunami of 26 December 2004: Numerical modeling and energy considerations-II, in *Tsunami and Its Hazard in Pacific and Indian Oceans*, *Pure Appl. Geophys.*, *164*(2/3), doi:10.1007/s00024-006-0162-7.

Lander, J. F., and P. A. Lockridge (1989), United States tsunamis 1690–1988, http://www.ngdc.noaa.gov/seg/hazard/tsu.shtml, Natl. Geophys. Data Cent., Boulder, Colo.

Lobkovsky, L. I., B. V. Baranov, R. K. Mazova, and L. Y. Kataeva (2006), Implications of the seismic source dynamics for the characteristics of a possible tsunami in a model problem of the seismic gap in the Central Kurile region, *Russ. J. Earth Sci.*, *8*, ES5002, doi:10.2205/2006ES000209.

Mader, C. L. (2004), *Numerical Modeling of Water Waves*, 274 pp., CRC Press, Boca Raton, Fla.

Mader, C. L., and E. N. Bernard (1993), Modeling tsunami flooding of Crescent City, paper presented at 16th IUGG/IOC International Tsunami Symposium, Int. Union of Geod. and Geophys., Wakayama, Japan.

Mei, C. C., M. Stiassnie, and D. K.-P. Yue (2005), *Theory and Applications of Ocean Surface Waves. Part 1: Linear Aspects*, *Adv. Ser. Ocean Eng.*, vol. 23, 506 pp., World Sci., Hackensack, N. J.

Mofjeld, H. O., V. V. Titov, F. I. Gonzalez, and J. C. Newman (2000), Analytic theory of tsunami wave scattering in the open ocean with application to the North Pacific, *NOAA Tech. Memo. OAR PMEL–116*, 38 pp., NOAA, Silver Spring, Md.

Okada, Y. (1985), Surface deformation due to shear and tensile faults in a half-space, *Bull. Seismol. Soc. Am.*, *75*, 1135–1154.

Reid, R. O., and R. O. Bodine (1968), Numerical model for storm surges in Galveston Bay, *J. Waterw. Harbors Coastal Eng. Div. Am. Soc. Civ. Eng.*, *94*, 33–57.

Roberts, J. A., and E. K. Kauper (1964), The effects of wind and precipitation on the modification of South Beach, Crescent City, California, Including an appendix on the focusing of tsunami energy at Crescent City, prepared by C.-W. Chien, final report, 98 pp., Environ. Sci. Div., Dep. of the Army, Washington, D. C.

Snodgrass, F. E., W. H. Munk, and G. R. Miller (1962), California's continental borderland. Part I. Background spectra, *J. Mar. Res.*, *20*, 3–30.

Titov, V., A. B. Rabinovich, H. O. Mofjeld, R. E. Thomson, and F. I. Gonzales (2005), The Global reach of the 26 December 2004 Sumatra Tsunami, *Science*, *309*, 2045–2048.

Wiegel, R. L. (1965), Protection of Crescent City California from tsunami waves, report, 112 pp., Redev. Agency of the City of Crescent City, Calif., Crescent City.

Yanuma, T., and Y. Tsuji (1998), Observation of edge waves trapped on the continental shelf in the vicinity of Makurazaki Harbor, Kyushu, Japan, *J. Oceanogr.*, *54*, 9–18.

J. Horrillo and Z. Kowalik, Institute of Marine Science, University of Alaska Fairbanks, Fairbanks, AK 99775, USA. (ffzk@ims.uaf.edu)

W. Knight, West Coast and Alaska Tsunami Warning Center, Palmer, AK 99645, USA.

T. Logan, Arctic Region Supercomputing Center, University of Alaska Fairbanks, Fairbanks, AK 99775, USA.